www.nature.com/cdd

CDDpress

ARTICLE

Check for updates

USP11 regulates autophagy-dependent ferroptosis after spinal cord ischemia-reperfusion injury by deubiquitinating Beclin 1

Yuluo Rong[1,2], Jin Fan[1,2], Chengyue Ji[1,2], Zhuanghui Wang[1], Xuhui Ge[1], Jiaxing Wang[1], Wu Ye[1], Guoyong Yin[1], Weihua Cai[1]✉ and Wei Liu[1]✉

Spinal cord ischemia-reperfusion injury (SCIRI) is a serious trauma that can lead to loss of sensory and motor function. Ferroptosis is a new form of regulatory cell death characterized by iron-dependent accumulation of lipid peroxides. Ferroptosis has been studied in various diseases; however, the exact function and molecular mechanism of ferroptosis in SCIRI remain unknown. In this study, we demonstrated that ferroptosis is involved in the pathological mechanism of SCIRI. Inhibition of ferroptosis could promote the recovery of motor function in mice after SCIRI. In addition, we found that ubiquitin-specific protease 11 (USP11) was significantly upregulated in neuronal cells after hypoxia-reoxygenation and in the spinal cord in mice with I/R injury. Knockdown of USP11 in vitro and KO of USP11 in vivo (*USP11*$^{-/Y}$) significantly decreased neuronal cell ferroptosis. In mice, this promotes functional recovery after SCIRI. In contrast, in vitro, USP11 overexpression leads to classic ferroptosis events. Overexpression of USP11 in mice resulted in increased ferroptosis and poor functional recovery after SCIRI. Interestingly, upregulating the expression of USP11 also appeared to increase the production of autophagosomes and to cause substantial autophagic flux, a potential mechanism through which USP11 may enhance ferroptosis. The decreased autophagy markedly weakened the ferroptosis mediated by USP11 and autophagy induction had a synergistic effect with USP11. Importantly, USP11 promotes autophagy activation by stabilizing Beclin 1, thereby leading to ferroptosis. In conclusion, this study shows that ferroptosis is closely associated with SCIRI, and that USP11 plays a key role in regulating ferroptosis and additionally identifies USP11-mediated autophagy-dependent ferroptosis as a promising target for the treatment of SCIRI.

Cell Death & Differentiation (2022) 29:1164–1175; https://doi.org/10.1038/s41418-021-00907-8

INTRODUCTION

Spinal cord ischemic-reperfusion injury (SCIRI) refers to a serious disease that can lead to severe sensory and motor dysfunction [1]. SCIRI occurs primarily in spinal trauma, spinal degeneration, and intraspinal tumors, and is also a common complication after thoracic and abdominal aortic surgery [2, 3]. If SCIRI is not treated in time, spinal cord function may incur long-term or permanent damage [4]. Therefore, studying the molecular and cellular mechanisms of SCIRI and identifying feasible and applicable treatments are particularly important.

Ferroptosis is a new form of programmed cell necrosis, which is different from apoptosis, necrosis, and autophagy in terms of morphology, biochemistry, and genetics [5, 6]. Ferroptosis essentially is oxidative damage caused by intracellular iron-induced reactive oxygen species (ROS) accumulation and lipid peroxidation, characterized by glutathione (GSH) depletion, GPX4 inactivation, and ultimately iron-dependent lipid peroxide accumulation [7]. Studies have shown that ferroptosis is widespread in various pathological processes such as cancer, degenerative diseases of the nervous system, and acute kidney injury [8–10]. Ferroptosis has also been reported in animal models of traumatic spinal cord injury and the inhibition of ferroptosis can promote functional recovery [11–13]. In addition, ferroptosis is involved in the organ damage induced by I/R, and inhibition of ferroptosis has been demonstrated to be effective against I/R-induced organ damage in a variety of experimental models [14–16]. However, the relevance of ferroptosis in SCIRI has not been explored and deserves further investigation.

Posttranslational modifications include ubiquitination, regulation of protein degradation, and membrane transport [17]. Ubiquitin-specific protease 11 (USP11) is a deubiquitinase (DUB) that is highly expressed in the human brain. Chiang et al. [18] have demonstrated the role of USP11-mediated SOX11 stabilization in cortical development, thus providing an explanation for the association between USP11 mutations and neurological disorders, and highlighting the importance of protein stabilization triggered by DUBs during development. Although USP11 has been investigated in many reports, the functional role of USP11 in neuroscience, particularly its role in SCIRI, has not been studied.

In this study, we provide the first clarification of the molecular mechanism and signaling pathway of ferroptosis in SCIRI. We found that ferroptosis is closely associated with SCIRI and USP11 plays a key role in regulating ferroptosis. The upregulation of USP11 induced by I/R triggers autophagy activation by stabilizing Beclin 1, promotes the degradation of autophagic ferritin, and ultimately leads to iron-dependent ferroptosis. In short, our study indicates that USP11 plays a significant role in the pathogenesis of

[1]Department of Orthopaedics, First Affiliated Hospital of Nanjing Medical University, Nanjing 210029 Jiangsu, China. [2]These authors contributed equally: Yuluo Rong, Jin Fan, Chengyue Ji. ✉email: caiwhspine@sina.com; liuweiorth@njmu.edu.cn

Edited by L Scorrano

Received: 12 July 2021 Revised: 13 November 2021 Accepted: 16 November 2021
Published online: 27 November 2021

ferroptosis in SCIRI; therefore, USP11 may be a potential target for the treatment of SCIRI.

MATERIALS AND METHODS

Animals

USP11$^{-/Y}$ (C57BL/6J background) mice were generated at Cyagen Biosciences (Cyagen Biosciences, Guangzhou, China). In this study, USP11 knockout (KO) mice were defined as *USP11*$^{-/Y}$ mice and *USP11*$^{+/Y}$ mice were defined as the control group. Supplementary Fig. S4A provides an overview of the target strategy. The two loxP sequences were inserted into introns one and nine of the USP11 gene with CRISPR-Cas9 to generate the conditional allele. The USP11 gene (NCBI reference sequence: NM_145628; Ensembl: ENSMUSG00000031066) is located on mouse chromosome X. A total of 21 exons were identified, with the ATG start codon in exon 1 and the TAA stop codon in exon 21 (transcript: ENSMUST00000033383). Exons 2–9 were selected as the target site. Cas9 and gRNA were co-injected into fertilized eggs for KO mouse production. The pups were genotyped by PCR and subjected to sequencing analysis.

SCIRI model

As described previously [19], the mouse SCIRI model was established in 6- to 8-week-old C57BL/6 male mice. The study was approved by the Ethics Committee of Nanjing Medical University. All procedures were performed in accordance with the guidelines of the National Institutes of Health Animal Laboratory Animal Care and Use Guidelines. In brief, mice were anesthetized by isoflurane inhalation and fixed in a supine position, and a midline abdominal incision method was used. After positioning of the left kidney through the peritoneum, we carefully searched for and separated the abdominal aorta along the left renal artery. The abdominal aorta was clamped under the exit of the left renal artery (which was not clamped in sham-operated mice). After 60 min, the aneurysm clip was removed and blood perfusion was restored. After the operation, the mice were placed in a cage alone and kept warm, and the bladder was massaged once every 8 h until the bladder reflex was restored.

Functional behavior analysis

The mice were kept under a 12 h light–dark cycle and given free access to food and water. Before the behavioral tests, all mice were acclimated with the test room or instrument for 1 h.

From the first day after SCI, Basso Mouse Scale (BMS) scores were used to analyze the neurological function of the mice at a fixed time point.

The inclined plane test was performed on testing equipment as previously described [20]. The maximum extent for which the mouse maintained the posture for at least 5 s was recorded.

We used a rotating rod that accelerated from 0 to 40 r.p.m. to assess overall athletic ability and coordination. Each mouse performed one test and then two tests with an interval of 20 min between tests. The average decrease in latency for the two trials performed on each mouse was determined.

The footprint analysis was performed as described previously [21]. Front and rear paws were coated with blue and red dyes, respectively. Then mice were encouraged to walk in a straight line on white paper. The obtained footprint patterns were analyzed to assess the recovery of coordination ability.

Electromyography was used to evaluate the motor evoked potentials of mice on the 28th day after injury [22]. Stimulation electrodes were placed at the head end of the surgically exposed spinal cord, recording electrodes were placed at the flexor biceps femoris muscle, reference electrodes were inserted at the tendons of the distal hind limb muscles, and grounding electrodes were placed under the skin.

Cell line and primary neuron culture

HEK 293T cells were purchased from the Cell Bank of the Chinese Academy of Sciences (Shanghai, China). Primary neuronal cells were cultured as described previously [20, 21]. Briefly, neurons were dissociated by digestion with 0.25% trypsin-EDTA solution (Thermo Fisher Scientific, MA, USA). After termination of the reaction, centrifugation was performed for 5 min (1000 r.p.m./min) at 4 °C to acquire cell suspensions. After being counted, cells were seeded on poly-L-lysine-coated culture plates and the medium was replaced with Neurobasal medium (Thermo Fisher Scientific) supplemented with 2% B27 (Gibco Laboratory, Grand Island, NY), 2 mM glutamine (Gibco) and 1% penicillin–streptomycin. Half the culture medium was exchanged every 2 days.

Oxygen glucose deprivation and reperfusion model

As described previously [23], an oxygen glucose deprivation and reperfusion (OGD/R) model was established to simulate SCIRI in vitro. In brief, the primary neurons were cultured in sugar-free medium, placed in a closed chamber, and then flushed with a continuous flow of mixed gas (95% N_2/5% CO_2) for 15 min. The chamber was then sealed and placed in a 37 °C incubator. After culturing for 60 min, the medium was replaced with normal medium and cells were placed in a normal incubator. Culturing continued for 0 to 2 h before further analysis.

Analysis of cell death and cell viability

Cell death was analyzed with propidiumiodide (PI) staining and microscopic analysis. Cell Counting Kit-8 (CCK-8) assays (Dojindo, Kumamoto, Japan) were used to assess cell viability. In brief, neuronal cells were plated in a 96-well plate. After specific treatment, 10 µl of CCK-8 reagent was added to each well and cells were incubated for 4 h at 37 °C under 5% CO_2. The absorbance was measured at 450 nm with an absorbance microplate reader (ELx800; Bio-Tek, USA).

Trypan blue staining

After specific treatment, the cells were mixed with trypan blue staining solution (Beyotime, China). After 3 min, the plates containing live cells (no cytoplasmic fluorescence) and dead cells (blue cytoplasmic fluorescence) were counted. ImageJ software (NIH, Bethesda, MD) was used to quantify the positive ratio of Trypan Blue from eight random fields.

Determination of lipid peroxidation, GSH, and iron content

According to the manufacturer's instructions, lipid peroxidation detection kits (ab118970 and ab238538, Abcam) were used to assess the concentrations of the lipid peroxidation products MDA and 4-HNE in cell lysates. A GSH assay kit (CS0260, Sigma) was used to assess the relative GSH concentration in cell lysates. An iron assay kit (ab83366, Abcam) was used to assess the relative iron concentration in cell lysates.

ROS analysis

According to a previous research method, the oxidation-sensitive fluorescent probe DCFH-DA was used to measure the level of ROS with a ROS Assay Kit (Beyotime, China) in the cells and then analyzed by flow cytometry (FACSCalibur; BD Biosciences).

Immunofluorescence staining

The cells or spinal cord sections were fixed with 4% paraformaldehyde for 10 min, permeabilized in 0.3% Triton X-100 for 10 min, blocked in 5% bovine serum albumin (BSA) for 1 h, and finally incubated with primary antibody overnight at 4 °C. Then the sections were incubated with secondary antibodies conjugated with Alexa Fluor 488 and Alexa Fluor 594 for 2 h at room temperature. Finally, the nuclei were counterstained with 4′,6-diamidino-2-phenylindole and images were obtained under the same exposure time and conditions.

Dihydroethidium staining

To assess the level of spinal cord oxidative stress, we incubated freshly prepared frozen spinal cord sections with the fluorescent dye dihydroethidium (DHE; Thermo Fisher Scientific, USA) at 2 µmol/L in a humidified chamber for 30 min at 37 °C, with protection from light. ImageJ software was used to quantify the red fluorescence intensity.

Reverse-transcription quantitative PCR

According to the manufacturer's instructions, SYBR Green Quantitative Polymerase Chain Reaction Kit (Qiagen, USA) was used to isolate total ribonucleic acid and perform quantitative PCR (qPCR). The ACTB level was used for normalization and the 2^{-ddCt} method was used to analyze the relative gene expression.

Plasmids and adenoviral infection

Cells were infected with adenovirus shRNA-control (Ad-shCtrl), adenovirus shRNA-ATG5, shRNA-USP11 or shRNA-Beclin 1 (Ad-shATG5, Ad-shUSP11, or

Ad-shBeclin 1), adenovirus vector (Ad-Vec), and adenovirus USP11 or adenovirus Beclin 1 (Ad-USP11 or Ad-Beclin 1). Full-length sequences for human USP11, Beclin 1, and ubiquitin were subcloned into the EcoRI and NotI sites of Flag-, Myc-, and HA tagged pcDNA3.1 vectors (Thermo Fisher Scientific).

Transmission electron microscopy

The treated neurons were incubated with a pre-chilled 2% glutaraldehyde solution for 2 h at 4 °C to fix the cell pellet. The cells were stained with 2% uranyl acetate solution for 2 h and then dehydrated in 50%, 70%, 90%, and 100% acetone. The cells were embedded and ultrathin sections were prepared for observation under an electron microscope (FEI Tecnai, Hillsboro, OR, USA).

Adeno-associated virus infection

To increase exogenous expression of USP11 in vivo, pAAV-PHP.eB-hSyn-USP11-3×FLAG-WPRE (AAV-USP11) was used (Obio Technology, Shanghai, China), and pAAV-PHP.eB-hSyn-3×FLAG-WPRE was used as a control vector (AAV-Con). AAV-PHP.eB vectors for expression of a short hairpin RNA directed at Beclin 1 (AAV-shBeclin 1) or a control hairpin (AAV-shCon) were generated for local depletion of Beclin 1 in vivo. The AAV-PHP.eB vector diluted in 0.9% sodium chloride to a final volume of 250 µL with a final titer of 3×10^{11} viral genome was injected into each mouse through the tail vein immediately after SCIRI.

Double-labeled adenovirus mRFP-GFP-LC3 transfection

The primary neurons prepared as described above were inoculated on a confocal culture dish for 4 days and then transfected with mRFP-GFP-LC3 adenovirus (Hanbio, China) according to the manufacturer's protocol. The treated cells were washed with phosphate-buffered saline, fixed in 4% paraformaldehyde, and observed under a confocal microscope.

Antibodies

The antibodies used for immunofluorescence were anti-USP11 (1 : 200, Santa Cruz Biotechnology), anti-GFAP (1 : 200, Cell Signaling Technology), anti-CD11b (1 : 200, Abcam), anti-NeuN (1 : 400, Abcam), and anti-CD31 (1 : 200, BD Biosciences). The antibodies used for western blotting were anti-Beclin 1 (1 : 2000, Proteintech), anti-USP11 (1 : 500, Santa Cruz Biotechnology), anti-GAPDH (1 : 2000, Servicebio), anti-NRF2 (1 : 2000, Cell Signaling Technology), anti-Flag-Tag (1 : 2000, Cell Signaling Technology), anti-GPX4 (1 : 5000, Abcam), anti-Myc-Tag (1 : 2000, Cell Signaling Technology), anti-FTH1 (1 : 2000, Abcam), anti-Myc-Tag (1 : 2000, Cell Signaling Technology), and anti-ACSL4 (1 : 10,000, Abcam).

Western blot analysis

Total protein was extracted from cells and tissues, and the protein concentration was measured with BCA assays (Beyotime, China). The proteins were separated by SDS-polyacrylamide gel electrophoresis and transferred to a polyvinylidene difluoride membrane. The membrane was blocked with 5% BSA at room temperature for 1 h and incubated with the primary antibody overnight at 4 °C. Then the membrane was incubated with horseradish peroxidase-conjugated anti-rabbit IgG and anti-mouse IgG (1 : 3000, Thermo Fisher Scientific, USA) for 120 min. Subsequently, an enhanced chemiluminescence reagent (Thermo Fisher Scientific, USA) was used to visualize immunolabeled bands. ImageJ was used to determine the protein expression level.

Immunoprecipitation

The cells were collected and an appropriate amount of cell immunoprecipitation (IP) lysis buffer containing protease inhibitors (Beyotime) was added. The cells were lysed on ice or at 4 °C for 30 min and the supernatant was extracted after centrifugation at $12{,}000 \times g$ for 30 min. A small amount of lysate was collected for western blot analysis, and the indicated antibodies and protein A/G-beads (Santa Cruz Biotechnology) were added to the remaining lysate, slowly shaken, and incubated at 4 °C overnight. After IP reaction, protein A/G-beads were centrifuged at 4 °C at $3000 \times g$ for 5 min. Protein A/G-beads were centrifuged to the bottoms of the tubes. The supernatant was carefully removed and protein A/G-beads were washed four times with lysis buffer. Finally, the bound protein was eluted by boiling and western blot analysis was performed.

IP coupled with mass spectrometry

Total proteins were extracted from the neurons and IP was performed with the indicated antibodies and Protein A/G-agarose beads (Santa Cruz Biotechnology) as described above. Then mass spectrometry (MS; Thermo Scientific, CA) was performed to analyze the isolated immunoprecipitates.

Statistical analyses

The data are shown as mean ± SD of at least three independent experiments. Statistical analysis was performed in GraphPad software 8.0 (GraphPad Software, La Jolla, CA). Unpaired two-tailed Student's *t*-test was used for comparison between two groups, one-way or two-way analysis of variance was used for comparisons among more than two groups, and then Tukey's post hoc test was used. A P-value < 0.05 was considered statistically significant.

RESULTS

USP11 is elevated in neuronal cell ferroptosis

We performed OGD/R treatment on neuronal cells and used the ferroptosis activator Erastin (5 µM, 6 h) as a positive control. The cell viability decreased significantly after OGD/R treatment (Fig. S1A). Trypan blue staining and PI staining showed that the live cells decreased sharply (Fig. S1B). GSH depletion, lipid peroxidation, and Fe^{2+} accumulation are the key events of ferroptosis. As expected, after OGD/R treatment, ferroptosis events were significantly triggered (Fig. S1C–F). Like Erastin treatment, OGD/R treatment resulted in a significant increase in ROS levels (Fig. S1G, H). In addition, the OGD/R and Erastin treatment showed an increase in the expression of ACSL4. Simultaneously, the levels of GPX4 and FTH1 decreased (Fig. S1I, J). Next, we treated neuronal cells with Liproxstatin-1, a potent and specific inhibitor of ferroptosis that has been shown to decrease I/R injury [10, 14]. Liproxstatin-1 inhibited the ferroptosis events induced by OGD/R (Fig. S1K–N). In CCK-8 detection and PI staining, we observed that liproxstatin-1 decreased the cell death (Fig. S1O, P). Therefore, we demonstrated that in neuronal cells, OGD/R damage can cause ferroptosis.

To further study the mechanism underlying neuronal cell ferroptosis, we performed microarray analysis and found that USP11 significantly increased after neuronal cell ferroptosis (data not shown). The upregulation mRNA expression of USP11 was then determined and confirmed by qPCR (Fig. S2A, D). After OGD/R and Erastin treatment, the protein level of USP11 was also increased significantly (Fig. S2B, C, E, F). We next predicted, on the basis of the online database (brainrnaseq.org), that USP11 would be highly expressed in neuronal cells (Fig. S2G). Immunofluorescence further showed that USP11 is mainly expressed in neuronal cells (Fig. S2H). Together, these results indicated that upregulated USP11 may play a key role in neuronal cell ferroptosis induced by I/R.

Ferroptosis occurs after SCIRI and the expression of USP11 is increased in vivo

Next, we further tested whether ferroptosis occurred after SCIRI. Western blotting showed higher levels of ACSL4 and lower levels of GPX4 and FTH1 after I/R, and these effects enhanced with increasing I/R duration (Fig. 1A–D). qPCR further confirmed the above results (Fig. 1E–G). Next, the relative values of GSH, MDA, and Fe^{2+} were also evaluated. With increasing I/R time, GSH decreased, and MDA and Fe^{2+} levels increased (Fig. 1H–J). In addition, as the I/R duration increased, the DHE intensity in the injured spinal cord increased (Fig. 1K). Next, we administered liproxstatin-1 to mice to determine the role of ferroptosis inhibition in SCIRI. Liproxstatin-1 induced GPX4 and FTH1 expression and decreased ACSL4 expression (Fig. S3A–D). Meanwhile, liproxstatin-1 inhibited oxidative stress in vivo (Fig. S3E). In addition, functional behavior analysis (BMS score, footprint analysis, and rotating rod test) and NeuN staining indicated that

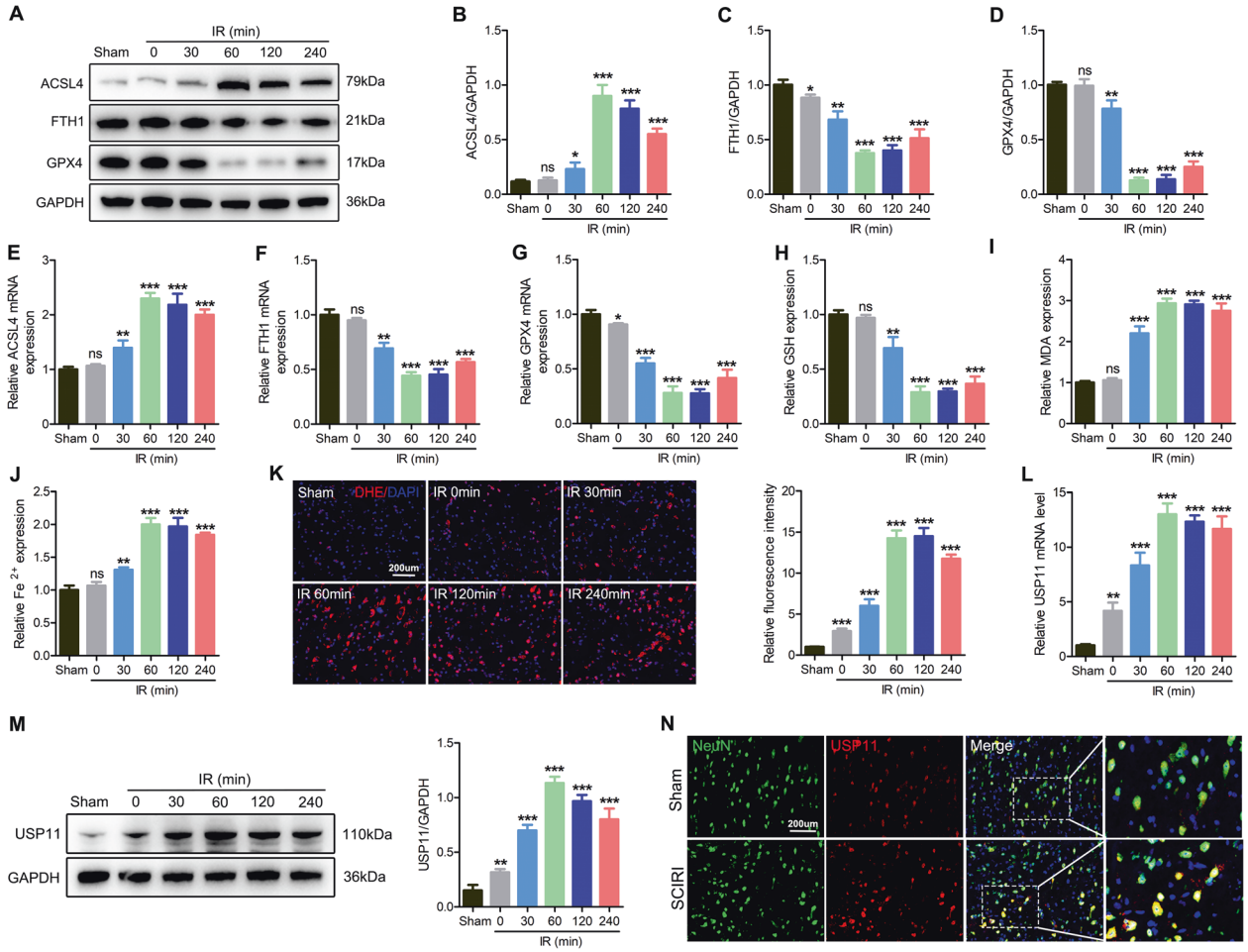

Fig. 1 Ferroptosis occurs after SCIRI, and the expression of USP11 increases. The spinal cord was subjected to I/R (I: 60 min; R: 0, 30, 60, 120, or 240 min) or sham surgery (sham). **A**–**D** Western blotting was used to detect the expression of ferroptosis-associated proteins at different time points after spinal cord I/R ($n = 3$). **E**–**G** qPCR was used to detect the mRNA expression of ferroptosis-associated proteins at different time points of spinal cord I/R ($n = 3$). **H**–**J** The relative values of GSH, MDA, and Fe^{2+} concentrations in injured spinal cord were determined ($n = 6$). **K** DHE staining was used to detect ROS levels in the injured spinal cord ($n = 6$). **L** The mRNA level of USP11 in the injured spinal cord was detected by qPCR ($n = 3$). **M** The protein expression of USP11 in the injured spinal cord was detected by western blotting ($n = 3$). **N** The expression of USP11 after spinal cord I/R (I: 60 min; R: 60 min) was analyzed by immunofluorescence. $^{*}P < 0.05$; $^{**}P < 0.01$; $^{***}P < 0.001$ compared with the sham group.

the inhibition of ferroptosis promoted the functional recovery after SCIRI and increased the number of surviving neurons (Fig. S3F–J).

In addition, we verified in vivo that USP11 may play a key role in regulating ferroptosis. We analyzed the mRNA and protein levels of USP11 after SCIRI. Interestingly, with increasing I/R duration, the expression levels of USP11 protein and mRNA increased (Fig. 1L–N). In summary, these results indicated that spinal cord I/R induces ferroptosis and increases the expression of USP11. Our findings suggest that USP11 may be involved in the activation of ferroptosis after SCIRI.

Increased expression of USP11 promotes ferroptosis

To determine whether the upregulated USP11 might be directly involved in the induction of ferroptosis, we pretreated neuronal cells with Ad-shUSP11 or Ad-USP11. Western blotting confirmed that Ad-shUSP11 significantly decreased, whereas Ad-USP11 significantly increased, the level of USP11 protein (Fig. 2A). In addition, we found that Ad-USP11 aggravated ferroptosis events (Fig. 2B–F). In contrast, knockdown of USP11 reversed these effects (Fig. 2B–F). Western blotting also confirmed that Ad-USP11 increased ACSL4 and decreased GPX4 and FTH1 (Fig. 2G). Next, knockdown of USP11 eliminated the partial viability inhibition, whereas overexpression of USP11 further decreased cell viability (Fig. 2H–K). Collectively, these findings indicated that increased USP11 expression leads to ferroptosis in neuronal cells.

KO of USP11 decreases ferroptosis and promotes functional recovery after SCIRI

We next used USP11 KO mice, denoted $USP11^{-/Y}$, to assess the consequences of USP11 physiological defects in vivo. USP11 was successfully knocked out in the spinal cord and primary cultured neuronal cells (Fig. S4B, C). In addition, $USP11^{+/Y}$ and $USP11^{-/Y}$ mice showed no significant differences in body weight and the number of neurons (Fig. S4D–F). BMS score and footprint analysis also showed that $USP11^{+/Y}$ and $USP11^{-/Y}$ mice had no significant differences in motor function (Fig. S4G–I). Overall, these results demonstrated that KO of USP11 does not affect normal spinal cord development and motor function in mice.

After SCIRI, the protein and mRNA expression of ACSL4 was lower in $USP11^{-/Y}$ mice than in $USP11^{+/Y}$ mice, whereas the protein and mRNA expression of the GPX4 and FTH1 was higher (Fig. 3A–D). In addition, the DHE intensity of the spinal cord in $USP11^{-/Y}$ mice also significantly decreased (Fig. 3E). After SCIRI, functional behavior analysis (BMS score, inclined plane tests, footprint analysis, and rotating rod test) indicated that the motor

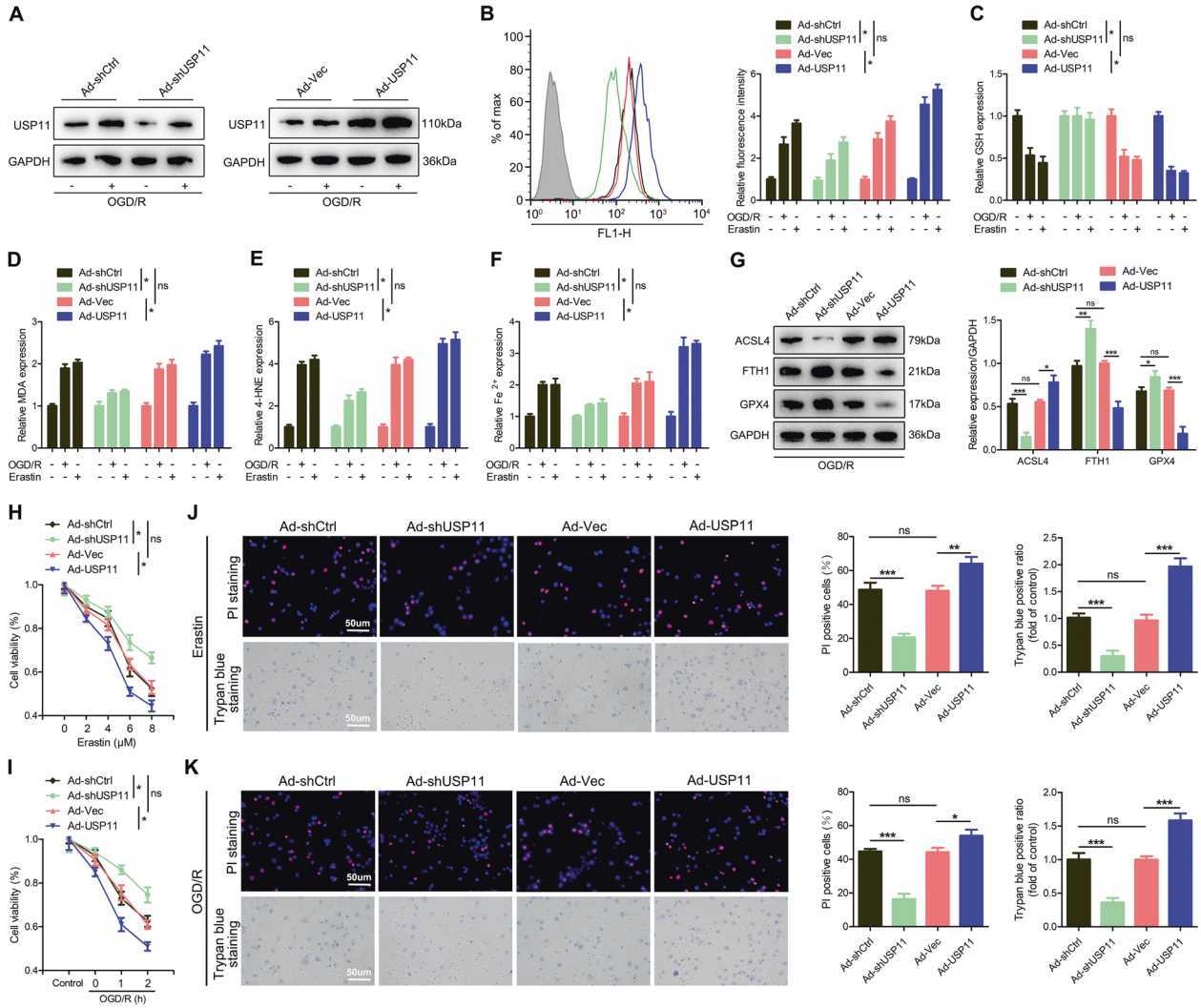

Fig. 2 USP11 promotes ferroptosis in vitro. The neuronal cells were transfected with Ad-shUSP11 or Ad-USP11, and then treated with Erastin (5 μM) for 6 h or OGD/R for 2 h. **A** The transfection efficiency was confirmed by western blot analysis ($n = 3$). **B**–**F** ROS, GSH, MDA, 4-HNE, and Fe^{2+} concentrations were measured ($n = 6$). **G** Western blot analysis was used to detect the expression of ferroptosis-associated proteins ($n = 3$). **H**, **I** CCK-8 was used to detect cell viability under Erastin or OGD/R treatment conditions ($n = 6$). **J**, **K** PI and trypan blue staining were used to detect cell survival under Erastin or OGD/R treatment conditions ($n = 6$). $^{*}P < 0.05$; $^{**}P < 0.01$; $^{***}P < 0.001$.

function recovery of *USP11*$^{-/Y}$ mice was significantly better than that of *USP11*$^{+/Y}$ mice (Fig. 3F–J). In addition, electromyography analysis showed that after SCIRI, compared with *USP11*$^{+/Y}$ mice, *USP11*$^{-/Y}$ mice had higher motor evoked potential amplitude and shorter latency (Fig. 3K, L). The number of surviving neuronal cells in the injured spinal cord area of *USP11*$^{-/Y}$ mice was significantly higher (Fig. 3M). In summary, the above results indicated that the lack of USP11 decreases ferroptosis and promotes the functional recovery after SCIRI.

Overexpression of USP11 promotes ferroptosis and impairs functional recovery after SCIRI

Then, we used the neuron cell-specific adeno-associated virus (AAV-PHP.eB-hSyn) for overexpression of USP11 after SCIRI. Western blotting showed that in sham-operated mice and SCIRI mice, injection of AAV-USP11 increased the expression of USP11 (Fig. S5A, B). The expression level of USP11 in the spinal cord was also evaluated by western blotting with anti-Flag antibody (Fig. S5C). In addition, immunofluorescence identified the specific expression of AAV-USP11 in neuronal cells in the spinal cord (Fig. S5D). Western blotting showed that after SCIRI, AAV-USP11 mice showed greater protein and mRNA expression of ACSL4, and decreased protein and mRNA expression of the GPX4 and FTH1 (Fig. S6A–D). In addition, the DHE intensity in the spinal cord in AAV-USP11 mice significantly increased (Fig. S6E). The BMS score, inclined plane test, and footprint analysis, rotating rod tests and electromyography analysis all showed that AAV-USP11 injection inhibited functional recovery in mice (Fig. S6F–L). Immunofluorescence showed that mice injected with AAV-USP11 had fewer surviving neurons (Fig. S6M). In summary, these results indicated that the neuronal cell-specific expression of USP11 promotes ferroptosis and hinders the recovery of function after SCIRI.

Ferroptosis promoted by USP11 is associated with autophagy activation

Previous studies have shown that ferroptosis is a process of autophagic cell death [24]. As expected, western blotting showed that USP11 silencing eliminated the transformation of LC3-I to LC3-II, whereas overexpression of USP11 enhanced the transformation of LC3-II (Fig. 4A). Overexpression of USP11 significantly increased the expression of Beclin 1, ATG5, and ATG7 (Fig. 4B, C). Next, we used several methods to evaluate the autophagic flux. First, western blotting and immunofluorescence showed that Ad-USP11 suppressed the protein expression of p62, whereas

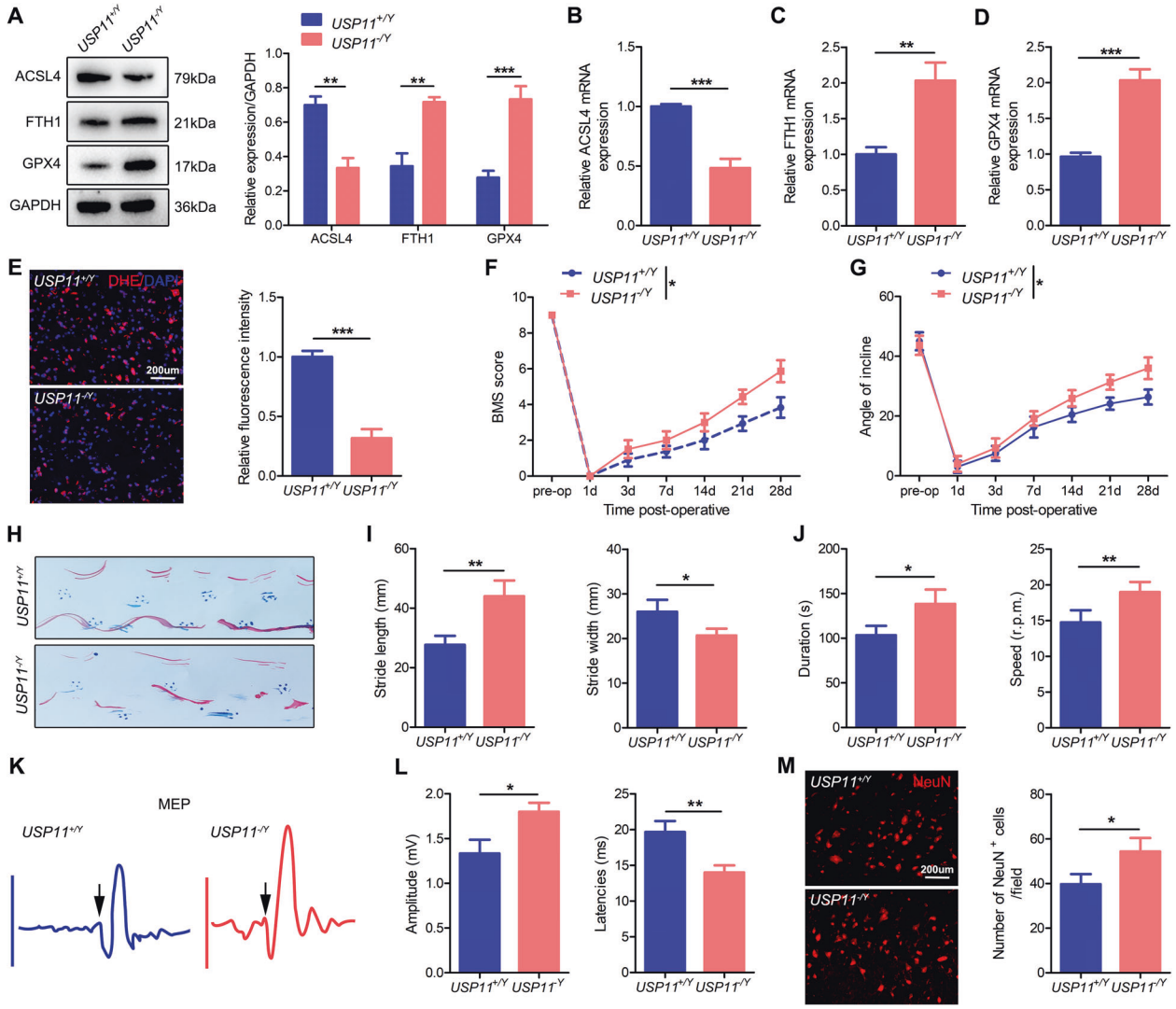

Fig. 3 Knockout of USP11 decreases ferroptosis and promotes functional recovery after SCIRI. A Representative western blot showing the expression of ferroptosis-associated proteins in the injured spinal cord (I: 60 min; R: 60 min) in $USP11^{+/Y}$ and $USP11^{-/Y}$ mice ($n = 3$). **B**–**D** mRNA levels of ferroptosis-associated proteins in injured spinal cord were detected by qPCR ($n = 3$). **E** DHE staining was used to detect ROS levels in the injured spinal cord ($n = 6$). **F**, **G** BMS and inclined plane test results on day 28 after SCIRI showed better functional recovery in $USP11^{-/Y}$ mice ($n = 8$). **H**–**J** Footprint and Rotarod test results on 28 day after SCIRI demonstrated better functional recovery of $USP11^{-/Y}$ mice ($n = 8$). **K**, **L** Electromyography analysis was used for electrophysiological assessment of $USP11^{+/Y}$ and $USP11^{-/Y}$ mice on day 28 after SCIRI ($n = 8$). **M** Representative immunofluorescence images of $NeuN^{+}$ neurons in the damaged spinal cord in $USP11^{+/Y}$ and $USP11^{-/Y}$ mice on day 28 after SCIRI ($n = 6$). $^{*}P < 0.05$; $^{**}P < 0.01$; $^{***}P < 0.001$.

Ad-shUSP11 increased the protein level of p62 (Fig. 4D, E). We then transfected neurons with mRFP-GFP-LC3 virus and observed autophagic flux. The number of autophagosomes and autophagolysosomes decreased after Ad-shUSP11 treatment, whereas pretreatment with Ad-USP11 resulted in a significant increase (Fig. 4F, G). Finally, autophagy was observed by transmission electron microscopy. Interestingly, after Ad-shUSP11 treatment, the presence of autophagosomes decreased, whereas pretreatment with Ad-USP11 resulted in a significant increase in autophagosomes (Fig. 4H, I). In addition, we inhibited autophagy both pharmacologically and genetically to further study Beclin 1-mediated autophagy-dependent ferroptosis regulated by USP11. Using the autophagy inhibitor chloroquine (CQ) or knocking down ATG5 to inhibit autophagy partially blocked the ferroptosis caused by Ad-USP11. Specifically, in the absence of Ad-USP11 or the presence of Ad-USP11, using CQ or knocking down ATG5 decreased the expression of ACSL4 and increased the levels of GPX4 and FTH1 (Fig. S7A, B, G, H). In addition, in the absence of Ad-USP11 or the presence of Ad-USP11, using CQ or knockdown of ATG5 decreased OGD/R-induced ferroptosis events (Fig. S7C–E, I–K). Simultaneously, the autophagy inhibitor CQ or ATG5 knockdown mediated inhibition of autophagy antagonized OGD/R-induced cell death (Fig. S7F, L). Overall, these data support the hypothesis that USP11 accumulation during ferroptosis triggers autophagy activation.

USP11 interacts with Beclin 1

To study the mechanism through which the accumulation of USP11 triggers autophagy activation during ferroptosis, we used IP coupled with MS (IP/MS) to study which proteins bind USP11. IP/MS identified Beclin 1 as a putative USP11 interacting protein (Fig. 5A). Co-IP analysis was performed to confirm the IP/MS results. As shown in Fig. 5B, USP11 precipitated Beclin 1 in neuronal cells, but NRF2 (another protein reported to bind USP11 and regulate ferroptosis) or control IgG did not precipitate. The interaction between USP11 and Beclin 1 was enhanced by OGD/R

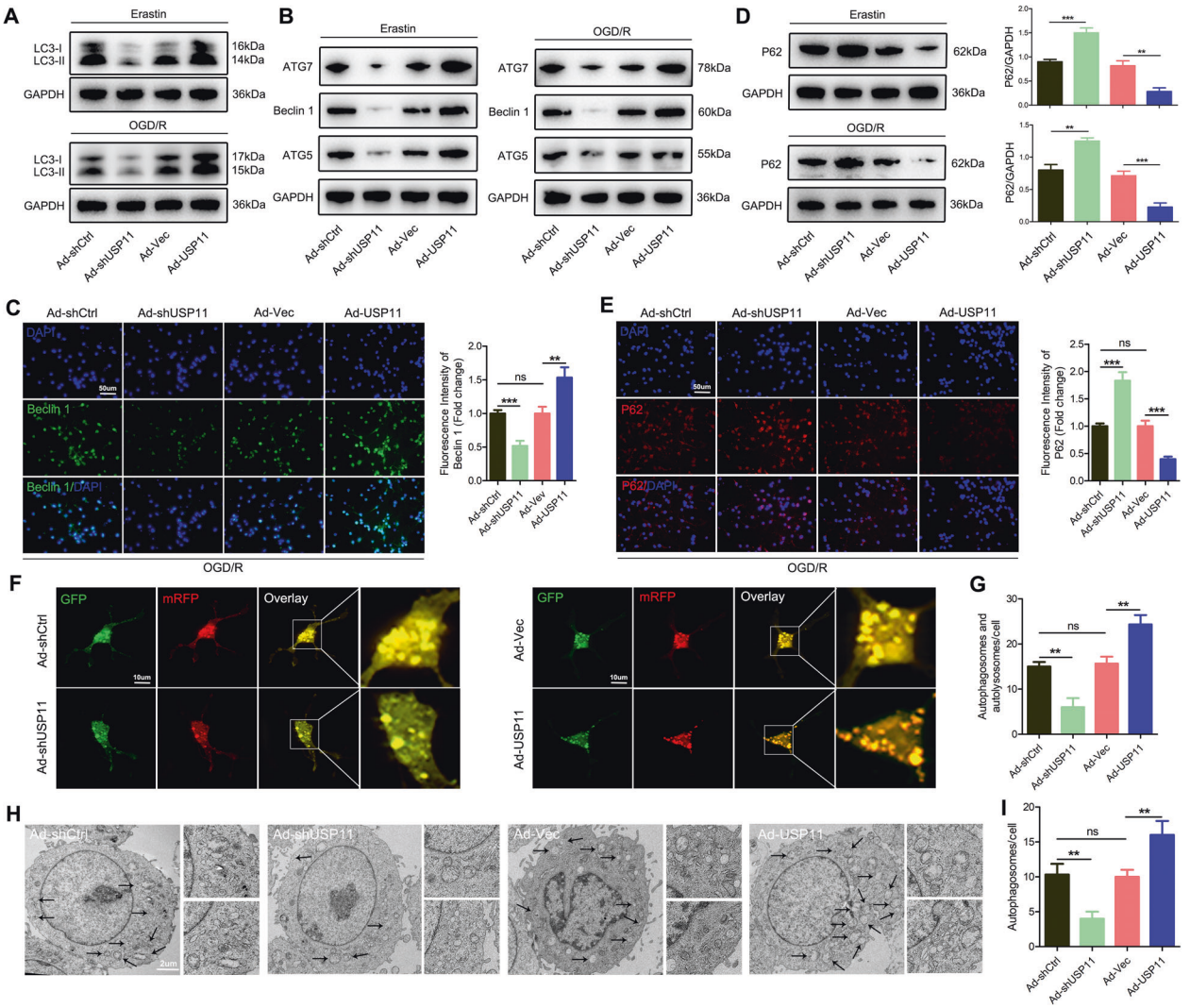

Fig. 4 Ferroptosis promoted by USP11 is associated with autophagy activation. Neuronal cells were transfected with Ad-shUSP11 or Ad-USP11, and then treated with Erastin (5 μM) for 6 h or OGD/R for 2 h. **A** Western blot analysis was used to determine the expression of LC3-I/II protein ($n = 3$). **B** Western blot analysis was used to detect the expression of autophagy-associated genes (ATG5, ATG7, and Beclin 1) ($n = 3$). **C** Immunofluorescence analysis of Beclin 1 protein expression ($n = 6$). **D**, **E** Western blot analysis and immunofluorescence were used to determine the expression of P62 protein ($n = 3$). **F**, **G** Confocal microscopy to detect the number of autophagosomes and autophagolysosomes after transfection of neurons with mRFP-GFP-LC3 adenovirus ($n = 6$). **H**, **I** Determination of autophagosomes by transmission electron microscopy analysis ($n = 6$). $^{**}P < 0.01$; $^{***}P < 0.001$.

treatment (Fig. 5C). Reverse Co-IP confirmed that USP11 was significantly precipitated by Beclin 1 in neuronal cells (Fig. 5D). We also performed a Co-IP test with epitope-tagged proteins in 293T cells. As expected, the Flag-labeled USP11 and Myc-labeled Beclin 1 co-precipitated efficiently in HEK 293T cells (Fig. 5E). These data demonstrate that USP11 interacts with Beclin 1. Using the full-length protein and a series of truncated Flag-labeled USP11 and Myc-labeled Beclin 1 fragments to detect the binding region in HEK 293T cells (Fig. 5F), we found that fragments containing amino acids 503–963 within the C terminus of USP11 was able to bind Beclin 1 (Fig. 5G). Further Co-IP analysis showed that USP11 was able to interact with only M2 plus the M3 domain of Beclin 1, but not the M1, M2, or M3 domain alone, thus indicating that the interaction may depend on the linkage region between the M2 and M3 domain (Fig. 5H).

USP11 inhibits Beclin 1 ubiquitination and degradation

Next, we studied the effect of USP11 silencing in neuronal cells on the expression level of Beclin 1. Compared with Ad-shCtrl, USP11 knockdown decreased the level of Beclin 1 protein but had no effect on the level of Beclin 1 mRNA, regardless of the presence or absence of either Erastin (Fig. S8A–C) or OGD/R treatment (Fig. S8D–F). This finding indicated that the regulation of Beclin 1 by USP11 does not occur at the mRNA level, but that the stability of Beclin 1 protein may be regulated by USP11. The addition of the proteasome inhibitor MG132 reversed the decline in Beclin 1 protein level after USP11 was depleted (Fig. 6A). We then investigated whether USP11 might stabilize Beclin 1. Overexpression of WT USP11 increased the level of Beclin 1 protein, whereas overexpression of the catalytically inactive C318A mutant USP11 did not cause such an increase (Fig. 6B). We next studied the effect of USP11 deletion on the stability of endogenous Beclin 1 protein in the presence of the protein synthesis inhibitor cycloheximide. Compared with that in control neuronal cells, the half-life of Beclin 1 protein in USP11 knockdown neuronal cells was shorter (Fig. 6C). Next, we sought to determine whether USP11 might regulate the ubiquitination and degradation of Beclin 1. Compared with Ad-shCtrl, USP11 knockdown effectively increased Beclin 1

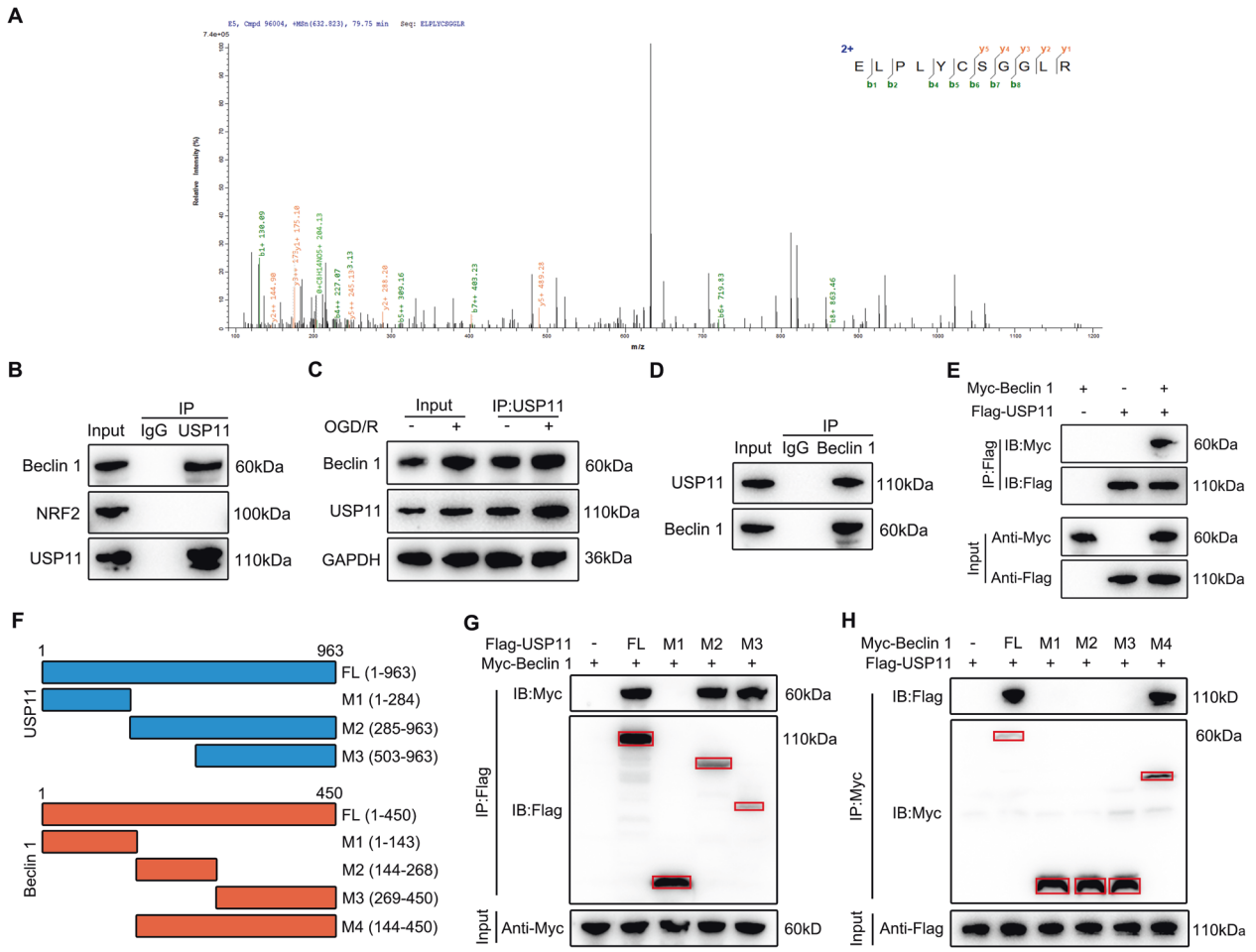

Fig. 5 USP11 interacts with Beclin 1. A IP/MS analysis was used to determine which proteins bind USP11, thus identifying Beclin 1 is an interacting protein. **B** Immunoprecipitation with anti-USP11 or anti-IgG was used to assess endogenous levels in neuronal cell lysate protein binding, and Beclin 1 and NRF2 were evaluated by immunoblotting with the indicated antibodies ($n = 3$). **C** After 2 h of OGD/R treatment in vitro, the same amount of protein lysate was immunoprecipitated with anti-USP11 antibody and used with the indicator ($n = 3$). **D** Immunoprecipitation with anti-Beclin 1 or anti-IgG was performed to confirm the endogenous protein interactions in neuronal cell lysates, and immunoblotting was performed with anti-USP11 ($n = 3$). **E** The lysate of HEK 293T cells transfected with Flag-labeled USP11 and Myc-labeled Beclin 1 was immunoprecipitated with anti-Flag, then immunoblotted with anti-Myc (Beclin 1) and anti-Flag (USP11) ($n = 3$). **F** Full-length (FL) USP11 with markers, schematic diagrams of FL Beclin 1 with Myc marker, and various deletion mutants. **G** HEK 293T cells were co-transfected with Myc-Beclin 1 and Flag-labeled FL or truncated USP11, and immunoprecipitated. The cell lysates were then assessed by anti-Myc and anti-Flag-labeled western blotting ($n = 3$). **H** HEK 293T cells were co-transfected with Flag-USP11 and Myc-labeled FL Beclin 1 or its deletion mutant, and the cell lysate was analyzed by immunoprecipitation. Immunoblot analysis was performed with anti-Flag and anti-Myc ($n = 3$). $^{*}P < 0.05$; $^{**}P < 0.01$; $^{***}P < 0.001$.

ubiquitination but decreased Beclin 1 protein levels (Fig. 6D). To confirm the effect of USP11 on Beclin 1 ubiquitination, we co-transfected HEK 293T cells with Myc-Beclin 1, Flag-USP11 (WT or C318A mutant), and HA-Ub. Overexpression of WT USP11 abolished the ubiquitination of Beclin 1 and this effect was reversed by the C318A mutant USP11 (Fig. 6E). In addition, Beclin 1 ubiquitination and degradation were significantly upregulated in the spinal cord in *USP11*$^{-/Y}$ mice compared with *USP11*$^{+/Y}$ mice, but were significantly lower after sham surgery or SCIRI than those in AAV-USP11-injected WT mice (Fig. 6F, G). We next studied the effect of USP11 on the polyubiquitin modification of Beclin 1 protein and found that USP11 cleaves the polyubiquitin chain associated with Lys48 but has no significant effect on the polyubiquitin chain associated with Lys63 (Fig. 6H). To confirm that Lys48-linked polyubiquitination is necessary for USP11-regulated Beclin 1 degradation, we expressed a Lys48-resistant (Lys48R) form of ubiquitin in USP11 knockdown HEK 293T cells and found that the expression of Lys48R ubiquitin eliminated the decrease in Beclin 1 induced by USP11 knockdown (Fig. 6I). Together, these data indicated that USP11 regulates the stability of Beclin 1 in neuronal cells and the spinal cord after SCIRI.

Inhibition of autophagy by Ad-shBeclin 1 decreases ferroptosis promoted by USP11

To study whether autophagy activation might mediate the enhanced ferroptosis of USP11, we used Ad-shBeclin 1 to block autophagy and used Ad-Beclin 1 to induce autophagy. Western blotting confirmed that Ad-shBeclin 1 not only decreased Beclin 1 levels but also significantly decreased the conversion rate of LC3-II (Fig. S9A). Figure S9B provides detailed information about the test groups in vitro. Then, in neuronal cells co-treated with Ad-shBeclin 1 and Ad-Beclin 1, we studied several typical ferroptosis events. Similarly, in the absence of Ad-USP11 or the presence of Ad-USP11, pretreatment with Ad-shBeclin 1 eliminated ferroptosis events (Fig. S9C, F–I). In contrast, compared with Ad-Beclin 1 alone, Ad-Beclin 1 and Ad-USP11 treatment resulted in an increase in ferroptosis events (Fig. S9C, F–I). Western blotting also confirmed that in the absence of Ad-USP11 or the presence of

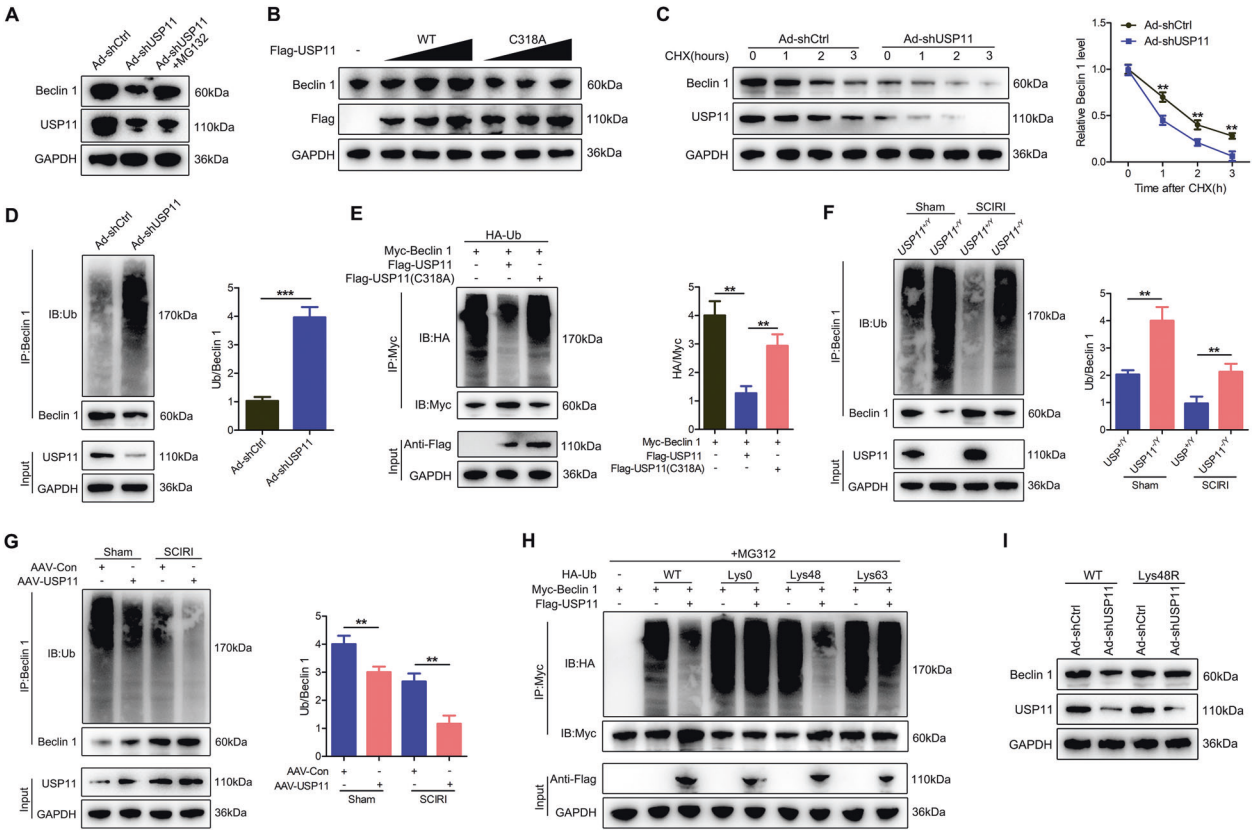

Fig. 6 USP11 inhibits Beclin 1 ubiquitination and degradation. A Analysis of Beclin 1 and USP11 in Ad-shUSP11-transfected neuronal cells with or without treatment with the proteasome inhibitor MG132 ($n = 3$). **B** Increasing Flag-tagged USP11 (WT or C318A mutant) was transfected into HEK 293T cells and the cell lysate was analyzed by immunoblotting with anti-Beclin 1 and anti-Flag ($n = 3$). **C** Beclin 1 protein levels in Ad-shCtrl and Ad-shUSP11 neurons were measured by western blotting targeting Beclin 1 and USP11 in the absence and presence of cycloheximide (CHX, 10 μg/mL) for a specified time ($n = 3$). **D** Lysates from Ad-shCtrl or Ad-shUSP11 transfected neuronal cells treated with MG132 before collecting were subjected to immunoprecipitation and detected with the indicated antibodies ($n = 3$). **E** The lysates of HEK 293T cells transfected with HA-labeled Ub and Myc-labeled Beclin 1, as well as Flag-labeled USP11 (WT) or Flag-labeled USP11 (C318A), were immunoprecipitated and subjected to anti-Myc immunoblotting followed by anti-HA and anti-Myc immunoblotting ($n = 3$). **F** Spinal cord lysates from *USP11*$^{+/Y}$ and *USP11*$^{-/Y}$ mice after SCIRI were immunoprecipitated with anti-Beclin 1 ($n = 6$). Ub-Beclin 1 was examined by immunoblotting with anti-Ub and anti-Beclin 1. **G** Spinal cord lysates from mice injected with AAV-Con or AAV-USP11 were immunoprecipitated with anti-Beclin 1 ($n = 6$). Ub-Beclin 1 was detected by western blotting with anti-Ub and anti-Beclin 1. **H** HEK 293T cells were co-transfected with Myc-Beclin 1, Flag-USP11 and HA-Ub Lys0, Lys48 alone, or Lys63 alone plasmids, and then Beclin 1 ubiquitination was analyzed ($n = 3$). **I** In the presence of Ad-shCtrl or Ad-shUSP11, HEK 293T cells transfected with either Ub WT or Ub Lys48R were cultured for 72 h. Cell lysates were analyzed by immunoblotting with anti-Beclin 1 and anti-USP11 ($n = 3$). $^{**}P < 0.01$; $^{***}P < 0.001$.

Ad-USP11, pretreatment with Ad-shBeclin 1 decreased ACSL4 and increased GPX4 and FTH1 (Fig. S9D, E).

In addition, knockdown of Beclin 1 resulted in resistance to Erastin or OGD/R-induced cell viability inhibition. In contrast, the upregulation of Beclin 1 expression significantly enhanced cell death induced by Erastin or OGD/R (Fig. S9J–M). Interestingly, in the presence of Ad-Beclin 1, Ad-USP11 showed a superimposed effect on the cell viability inhibition. However, in the presence of Beclin 1 knockdown, the overexpression of USP11 did not significantly promote the cell viability inhibitory effects (Fig. S9J–M), thus indicating that the accumulation of USP11 led to ferroptosis through an autophagy-dependent mechanism.

USP11 promotes ferroptosis and limits functional recovery by increasing Beclin 1 levels after SCIRI

The above results indicated that USP11 interacts with and stabilizes Beclin 1. We next investigated whether USP11 might selectively target Beclin 1, thereby causing ferroptosis and limiting functional recovery. We injected AAV-USP11 and AAV-shBeclin 1 or corresponding controls to generate mice with neuronal cell-specific USP11 overexpression and Beclin 1 knockdown. Figure 7A provides detailed information about the experimental group. Similarly to the above results (Fig. S6), these results indicated that, compared with AAV-Con after SCIRI, USP11 overexpression promoted ferroptosis, inhibited functional recovery, and decreased the number of surviving neurons (Fig. 7B–N; Group 2 vs. Group 1). These unfavorable effects were significantly inhibited in mice injected with AAV-Con and AAV-shBeclin 1, or in mice injected with AAV-USP11 and AAV-shBeclin 1 (Fig. 7B–N; Group 3 vs. Group 1, and Group 4 vs. Group 2). In summary, these data indicated that USP11 causes ferroptosis after SCIRI by increasing Beclin 1 levels, thus limiting functional recovery.

DISCUSSION

In the current study, we provide the first report that ferroptosis is involved in the pathogenesis of SCIRI. Inhibition of ferroptosis promoted the functional recovery of mice after SCIRI. In addition, we used the method of loss of function and gain of function to demonstrate the functional role of USP11 in regulating iron-dependent ferroptosis, which had not been reported before. USP11 triggers autophagy activation by stabilizing Beclin 1, promotes the degradation of autophagic ferritin, and ultimately

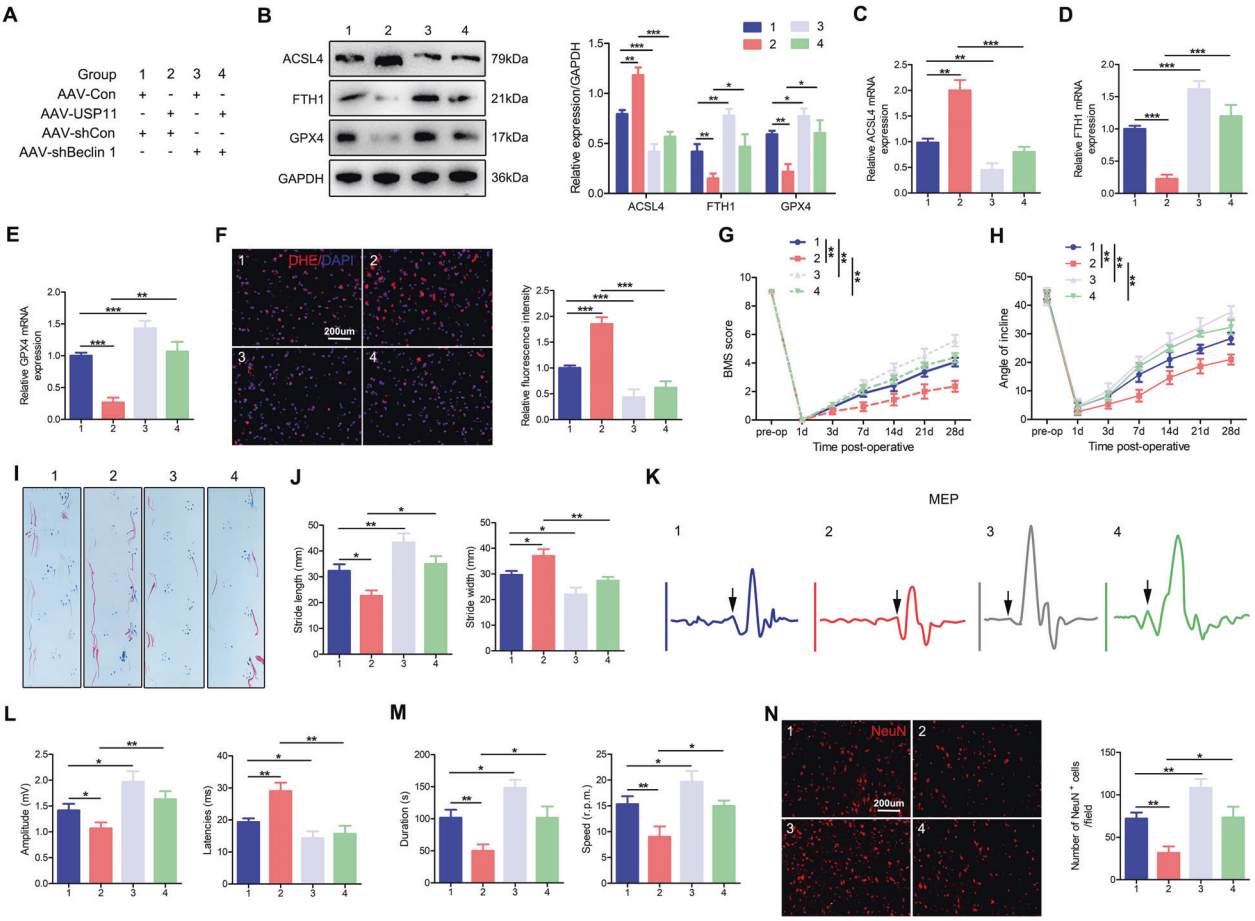

Fig. 7 USP11 promotes ferroptosis, thus limited functional recovery by increasing Beclin 1 levels after SCIRI. A Detailed information on the experimental group in this part of the experiment. **B** Representative western blot showing the protein expression of ferroptosis-associated proteins in the injured spinal cord in mice (I: 60 min; R: 60 min) ($n = 3$). **C**–**E** qPCR was used to detect the mRNA level of ferroptosis-associated proteins in the injured spinal cord ($n = 3$). **F** DHE staining was used to detect ROS levels in the injured spinal cord in mice ($n = 6$). **G**, **H** BMS scores and inclined plane test results after SCIRI ($n = 8$). **I**, **J** Footprint test results on day 28 after SCIRI ($n = 8$). **K**, **L** Electromyography analysis on day 28 after SCIRI as an electrophysiological evaluation (arrow indicates the onset of evoked potential) ($n = 8$). **M** Rotarod test on day 28 after SCIRI ($n = 8$). **N** Representative immunofluorescence images of $NeuN^+$-positive neurons in the area of the lesion on day 28 after SCIRI ($n = 6$). $^*P < 0.05$; $^{**}P < 0.01$; $^{***}P < 0.001$.

leads to iron-dependent ferroptosis. Therefore, we believe that USP11 may be a promising therapeutic target for the treatment of SCIRI.

Increasing evidence shows that the USP11 plays a key role in the regulation of neurodevelopmental disorders [18], DNA damage repair [25, 26], apoptosis regulation [27], and tumor regulation [28, 29]. Recently, Meng et al. [30] have reported that in non-small cell lung cancer, USP11 regulates cell proliferation and ferroptosis by stabilizing NRF2 protein. Therefore, DUBs may plausibly play an important role in the regulation of iron metabolism by modifying the proteins involved in the iron metabolism pathway. Microarray analysis showed that USP11 was upregulated after neuronal cell ferroptosis, although the exact biological function of USP11 after SCIRI remains unclear. To confirm our microarray results, we verified the expression of USP11 in vivo and found that after SCIRI, its expression increased significantly at both the mRNA and protein levels. Immunofluorescence staining showed that USP11 was mainly expressed in neuronal cells, thus indicating that USP11 plays a role in neuronal damage. We thus showed that the loss of USP11 significantly inhibits ferroptosis and promotes functional recovery, whereas overexpression of USP11 has opposite effects. In addition, we showed that SCIRI is closely associated with ferroptosis. I/R is clearly a dynamic process involving complex cell death mechanisms. However, the coordination of these cell death processes requires more in-depth research.

Interestingly, multiple studies have shown an important relationship between ferroptosis and autophagy [24, 31–33]. Autophagy is considered an upstream mechanism that induces ferroptosis by regulating cellular iron homeostasis and cellular reactive oxygen generation [24, 31]. In agreement with previous studies, we showed that upregulated USP11 expression increases autophagosome production and autophagic flux, a potential mechanism through which USP11 may enhance ferroptosis. To further study the mechanism through which USP11 accumulation triggers autophagy activation during ferroptosis, we performed IP/MS and determined that Beclin 1 protein interacts with USP11 in neuronal cells. Studies have shown that in colorectal cancer chemotherapy and liver cancer disease models, USP11 regulates the expression of mammalian target of rapamycin (mTOR) by stabilizing various downstream target proteins, thereby inhibiting or activating autophagy [34, 35]. However, in the neuronal cell OGD/R model, we found that USP11 did not affect the expression of AMPK, mTOR, and ULK1 proteins (data not shown), but directly activated autophagy by stabilizing Beclin 1. In addition, our experiments indicated that USP11 affected the expression of ATG5/7 protein, but the IP/MS experiment did not reveal the combination of USP11 and ATG5/7. Therefore, we speculate that

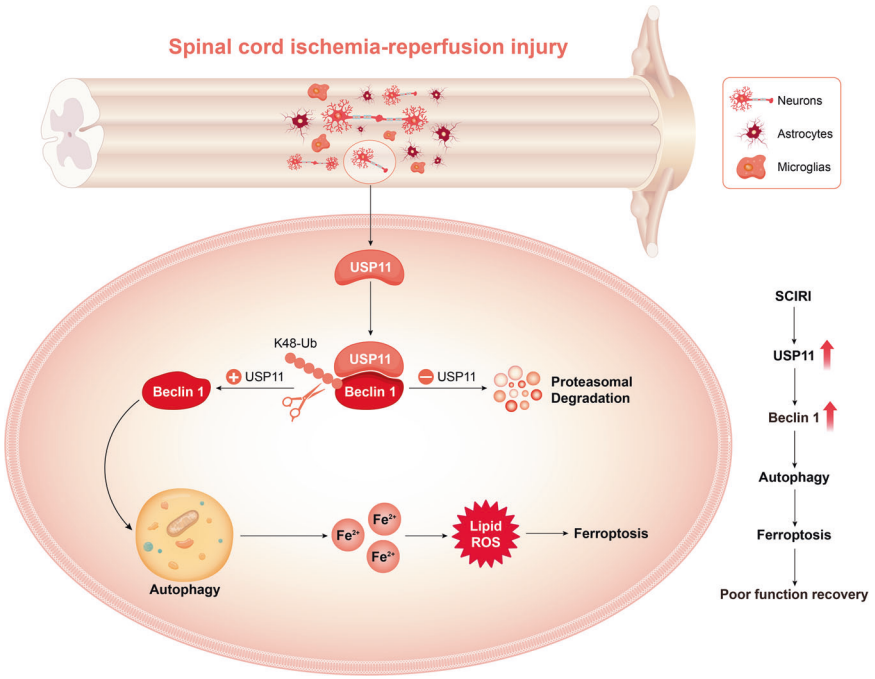

Fig. 8 USP11 regulates autophagy-dependent ferroptosis after spinal cord ischemia-reperfusion injury by deubiquitinating Beclin 1. The upregulation of USP11 induced by SCIRI triggers autophagy activation by stabilizing Beclin 1, promotes the degradation of autophagic ferritin, and ultimately leads to iron-dependent ferroptosis, thus resulting in poor functional recovery.

USP11 may indirectly regulate the expression of ATG5/7 through other means, but the specific mechanism requires further research.

Beclin 1 plays an important role in autophagy. Under physiological and pathological conditions, regulation of Beclin 1 may be an important mechanism to control autophagy. Sun et al. have recently confirmed that targeting Beclin 1 to induce autophagy may have a protective effect on the heart during sepsis [36]. In addition, Jin et al. [37] have reported that USP19 promotes autophagy and the antiviral immune response by deubiquitinating Beclin 1. In agreement with findings from previous studies, we showed that in neuronal cell ferroptosis, the autophagy activation of USP11 may occur through a Beclin 1-dependent mechanism. We also attempted to determine whether USP11 can be precipitated with antibodies to another protein, NRF2, which has been reported to be associated with ferroptosis. Our Co-IP results showed that USP11 did not interact with NRF2 in neuronal cells. We then tested the mRNA and protein levels of Beclin 1 in neuronal cells with knockdown of USP11. Interestingly, the down-regulation of USP11 significantly decreased the protein level of Beclin 1 but not at its mRNA level, thus indicating that posttranslational modifications may play important roles in regulating the stability of Beclin 1. Beclin 1 has been widely reported to be regulated by the ubiquitin-proteasome system in various disease models [38, 39]. Interestingly, another study has shown that USP14 regulates autophagy by inhibiting K63 ubiquitination of Beclin 1 [40]. Here we showed that USP11 interacts stably with Beclin 1 and eliminates Beclin 1 ubiquitination, thus decreasing Beclin 1 degradation in neuronal cells and damaged spinal cord. The depletion of Beclin 1 in vivo and in vitro also reverses ferroptosis enhanced by overexpression of USP11, thus indicating that the stability of Beclin 1 is essential for USP11's regulation of neuronal cell ferroptosis. These data indicate that USP11 may regulate neuronal cell ferroptosis by affecting the stability of Beclin 1. Of note, studies have shown that Beclin 1 can promote ferroptosis through regulating the activity of the cysteine and glutamate antiporter system xc− in cancer cells [41, 42]. Therefore, we inhibited autophagy both pharmacologically and genetically to further study Beclin 1-mediated autophagy-dependent ferroptosis regulated by USP11. Using the autophagy inhibitor CQ or knocking down ATG5 to inhibit autophagy partially blocked the ferroptosis caused by USP11 overexpression.

In summary, ferroptosis is closely associated with SCIRI. The interaction between USP11 and Beclin 1 is a key molecular event that triggers the activation of autophagy, promotes the degradation of autophagic ferritin, and leads to ferroptosis (Fig. 8). Understanding of the molecular mechanism and signaling pathways of ferroptosis may provide new diagnosis and treatment methods for regulating the survival and death of neuronal cells after SCIRI. Our results emphasize the importance of USP11-mediated Beclin 1 posttranslational regulation in neuronal cells. Targeting USP11 may be a promising treatment strategy for SCIRI. Further studies are also encouraged to develop USP11-specific antagonists for treating SCIRI.

DATA AVAILABILITY

Most datasets supporting the conclusions of this study are included within this article and the additional files. The datasets used or analyzed during the current study are available on reasonable request.

REFERENCES

1. Smith PD, Puskas F, Meng X, Lee JH, Cleveland JC Jr, Weyant MJ, et al. The evolution of chemokine release supports a bimodal mechanism of spinal cord ischemia and reperfusion injury. Circulation. 2012;126:S110–117. 11 Suppl 1.
2. Wynn MM, Acher CW. A modern theory of spinal cord ischemia/injury in thoracoabdominal aortic surgery and its implications for prevention of paralysis. J Cardiothorac Vasc Anesth. 2014;28:1088–99.
3. Bell MT, Puskas F, Agoston VA, Cleveland JC Jr, Freeman KA, Gamboni F, et al. Toll-like receptor 4-dependent microglial activation mediates spinal cord ischemia-reperfusion injury. Circulation. 2013;128:S152–156. 11 Suppl 1.
4. Guo X, Feng Y, Sun T, Feng S, Tang J, Chen L, et al. Clinical guidelines for neurorestorative therapies in spinal cord injury (2021 China version). J Neurorestoratol 2021;9:31–49.
5. Dixon SJ, Lemberg KM, Lamprecht MR, Skouta R, Zaitsev EM, Gleason CE, et al. Ferroptosis: an iron-dependent form of nonapoptotic cell death. Cell. 2012; 149:1060–72.

6. Chen X, Li J, Kang R, Klionsky DJ, Tang D. Ferroptosis: machinery and regulation. Autophagy. 2021;17:2054–81.
7. Xie Y, Hou W, Song X, Yu Y, Huang J, Sun X, et al. Ferroptosis: process and function. Cell Death Differ. 2016;23:369–79.
8. Stockwell BR, Jiang X, Gu W. Emerging mechanisms and disease relevance of ferroptosis. Trends Cell Biol. 2020;30:478–90.
9. Liang C, Zhang X. Recent progress in ferroptosis inducers for cancer therapy. Adv Mater. 2019;31:e1904197.
10. Friedmann Angeli JP, Schneider M, Proneth B, Tyurina YY, Tyurin VA, Hammond VJ, et al. Inactivation of the ferroptosis regulator Gpx4 triggers acute renal failure in mice. Nat Cell Biol. 2014;16:1180–91.
11. Chen Y, Liu S. The latest view on the mechanism of ferroptosis and its research progress in spinal cord injury. Oxid Med Cell Longev. 2020;2020:6375938.
12. Zhang Y, Sun C, Zhao C, Hao J, Zhang Y, Fan B, et al. Ferroptosis inhibitor SRS 16-86 attenuates ferroptosis and promotes functional recovery in contusion spinal cord injury. Brain Res. 2019;1706:48–57.
13. Yao X, Zhang Y, Hao J, Duan HQ, Zhao CX, Sun C, et al. Deferoxamine promotes recovery of traumatic spinal cord injury by inhibiting ferroptosis. Neural Regen Res. 2019;14:532–41.
14. Li Y, Feng D, Wang Z, Zhao Y, Sun R, Tian D, et al. Ischemia-induced ACSL4 activation contributes to ferroptosis-mediated tissue injury in intestinal ischemia/reperfusion. Cell Death Differ. 2019;26:2284–99.
15. Li Y, Cao Y, Xiao J, Shang J, Tan Q, Ping F, et al. Inhibitor of apoptosis-stimulating protein of p53 inhibits ferroptosis and alleviates intestinal ischemia/reperfusion-induced acute lung injury. Cell Death Differ. 2020;27:2635–50.
16. Yamada N, Karasawa T, Wakiya T, Sadatomo A, Ito H, Kamata R, et al. Iron overload as a risk factor for hepatic ischemia-reperfusion injury in liver transplantation: potential role of ferroptosis. Am J Transplant. 2020;20:1606–18.
17. Critchley WR, Pellet-Many C, Ringham-Terry B, Harrison MA. Receptor tyrosine kinase ubiquitination and de-ubiquitination in signal transduction and receptor trafficking. Cells 2018;7:22.
18. Chiang SY, Wu HC, Lin SY, Chen HY. Usp11 controls cortical neurogenesis and neuronal migration through Sox11 stabilization. Sci Adv. 2021;7:eabc6093.
19. Huang Y-F, Gu C-J, Wang Q, Xu L, Chen J, Zhou W, et al. The protective effort of GPCR kinase 2-interacting protein-1 in neurons via promoting Beclin1-Parkin induced mitophagy at the early stage of spinal cord ischemia-reperfusion injury. FASEB J. 2020;34:2055–74.
20. Rong Y, Liu W, Lv C, Wang J, Luo Y, Jiang D, et al. Neural stem cell small extracellular vesicle-based delivery of 14-3-3t reduces apoptosis and neuroinflammation following traumatic spinal cord injury by enhancing autophagy by targeting Beclin-1. Aging. 2019;11:7723–45.
21. Rong Y, Liu W, Wang J, Fan J, Luo Y, Li L, et al. Neural stem cell-derived small extracellular vesicles attenuate apoptosis and neuroinflammation after traumatic spinal cord injury by activating autophagy. Cell Death Dis. 2019;10:340.
22. Liu W, Ge X, Zhou Z, Jiang D, Rong Y, Wang J, et al. Deubiquitinase USP18 regulates reactive astrogliosis by stabilizing SOX9. Glia. 2021;69:1782–98.
23. Chen J, Wang Q, Zhou W, Zhou Z, Tang PY, Xu T, et al. GPCR kinase 2-interacting protein-1 protects against ischemia-reperfusion injury of the spinal cord by modulating ASK1/JNK/p38 signaling. FASEB J. 2018;fj201800548.
24. Gao M, Monian P, Pan Q, Zhang W, Xiang J, Jiang X. Ferroptosis is an autophagic cell death process. Cell Res. 2016;26:1021–32.
25. Deng T, Yan G, Song X, Xie L, Zhou Y, Li J, et al. Deubiquitylation and stabilization of p21 by USP11 is critical for cell-cycle progression and DNA damage responses. Proc Natl Acad Sci USA. 2018;115:4678–83.
26. Ting X, Xia L, Yang J, He L, Si W, Shang Y, et al. USP11 acts as a histone deubiquitinase functioning in chromatin reorganization during DNA repair. Nucleic Acids Res. 2019;47:9721–40.
27. Lee EW, Seong D, Seo J, Jeong M, Lee HK, Song J. USP11-dependent selective cIAP2 deubiquitylation and stabilization determine sensitivity to Smac mimetics. Cell Death Differ. 2015;22:1463–76.
28. Zhou Z, Luo A, Shrivastava I, He M, Huang Y, Bahar I, et al. Regulation of XIAP turnover reveals a role for USP11 in promotion of tumorigenesis. EBioMedicine. 2017;15:48–61.
29. Kapadia B, Nanaji NM, Bhalla K, Bhandary B, Lapidus R, Beheshti A, et al. Fatty acid synthase induced S6Kinase facilitates USP11-eIF4B complex formation for sustained oncogenic translation in DLBCL. Nat Commun. 2018;9:829.
30. Meng C, Zhan J, Chen D, Shao G, Zhang H, Gu W, et al. The deubiquitinase USP11 regulates cell proliferation and ferroptotic cell death via stabilization of NRF2 USP11 deubiquitinates and stabilizes NRF2. Oncogene. 2021;40:1706–20.
31. Hou W, Xie Y, Song X, Sun X, Lotze MT, Zeh HJ 3rd, et al. Autophagy promotes ferroptosis by degradation of ferritin. Autophagy. 2016;12:1425–8.
32. Zhang Z, Yao Z, Wang L, Ding H, Shao J, Chen A, et al. Activation of ferritinophagy is required for the RNA-binding protein ELAVL1/HuR to regulate ferroptosis in hepatic stellate cells. Autophagy. 2018;14:2083–103.
33. Latunde-Dada GO. Ferroptosis: role of lipid peroxidation, iron and ferritinophagy. Biochim Biophys Acta. 2017;1861:1893–1900.
34. Qiao L, Zhang Q, Sun Z, Liu Q, Wu Z, Hu W, et al. The E2F1/USP11 positive feedback loop promotes hepatocellular carcinoma metastasis and inhibits autophagy by activating ERK/mTOR pathway. Cancer Lett. 2021;514:63–78.
35. Sun H, Wang R, Liu Y, Mei H, Liu X, Peng Z. USP11 induce resistance to 5-fluorouracil in colorectal cancer through activating autophagy by stabilizing VCP. J Cancer. 2021;12:2317–25.
36. Sun Y, Yao X, Zhang QJ, Zhu M, Liu ZP, Ci B, et al. Beclin-1-dependent autophagy protects the heart during sepsis. Circulation. 2018;138:2247–62.
37. Jin S, Tian S, Chen Y, Zhang C, Xie W, Xia X, et al. USP19 modulates autophagy and antiviral immune responses by deubiquitinating Beclin-1. EMBO J. 2016;35:866–80.
38. Shi CS, Kehrl JH. Traf6 and A20 differentially regulate TLR4-induced autophagy by affecting the ubiquitination of Beclin 1. Autophagy. 2010;6:986–7.
39. Geisler S, Jäger L, Golombek S, Nakanishi E, Hans F, Casadei N, et al. Ubiquitin-specific protease USP36 knockdown impairs Parkin-dependent mitophagy via downregulation of Beclin-1-associated autophagy-related ATG14L. Exp cell Res. 2019;384:111641.
40. Xu D, Shan B, Sun H, Xiao J, Zhu K, Xie X, et al. USP14 regulates autophagy by suppressing K63 ubiquitination of Beclin 1. Genes Dev. 2016;30:1718–30.
41. Zhou B, Liu J, Kang R, Klionsky DJ, Kroemer G, Tang D. Ferroptosis is a type of autophagy-dependent cell death. Semin Cancer Biol. 2020;66:89–100.
42. Kang R, Zhu S, Zeh HJ, Klionsky DJ. BECN1 is a new driver of ferroptosis. Autophagy. 2018;14:2173–5.

AUTHOR CONTRIBUTIONS

WL, WC, and JF designed and supervised this study. YR and CJ conducted the majority of the experiments and completed the manuscript. ZW and GY analyzed the data. XG, JW, and WY participated in the experiments and manuscript writing. All authors approved the final version of the manuscript.

FUNDING

This work was sponsored by the National Natural Science Foundation of China (grant No. 81974335, 82172426).

COMPETING INTERESTS

The authors declare no competing interests.

ETHICS APPROVAL AND CONSENT TO PARTICIPATE

All animal procedures were performed under the guidelines of the institutional review board and the ethics committee of Nanjing Medical University.

ADDITIONAL INFORMATION

Supplementary information The online version contains supplementary material available at https://doi.org/10.1038/s41418-021-00907-8.

Correspondence and requests for materials should be addressed to Weihua Cai or Wei Liu.